PAPER

A photoluminescent and electrochemiluminescent probe based on an iridium(III) complex with a boronic acid-functionalised ancillary ligand for the selective detection of mercury(II) ions†

Kyoung-Rok Kim, Jinrok Oh and Jong-In Hong [ID] *

Exposure to mercury(II) ions (Hg^{2+}) can cause various diseases such as Minamata disease, acrodynia, Alzheimer's disease, and Hunter–Russell syndrome, and even organ damage. Therefore, real-time and accurate monitoring of Hg^{2+} in environmental samples is crucial. In this study, we report a photoluminescent (PL) and electrochemiluminescent (ECL) probe based on a cyclometalated Ir(III) complex for the selective detection of Hg^{2+}. The introduction of a reaction site, *o*-aminomethylphenylboronic acid, on the ancillary ligands allowed a prompt transmetalation reaction to take place between Hg^{2+} and boronic acid. This reaction resulted in significant decreases of the PL and ECL signals due to the photo-induced electron transfer from the Ir(III) complex to the Hg^{2+} ions. The probe was applied to the selective detection of Hg^{2+}, and the signal changes revealed a linear correlation with Hg^{2+} concentrations in the range of 0−10 μM (LOD = 0.72 μM for PL, 8.03 nM for ECL). The designed probe allowed the successful quantification of Hg^{2+} in tap water samples, which proves its potential for the selective detection of Hg^{2+} in environmental samples.

Introduction

Rapid industrialisation has resulted in the frequent release of toxic chemicals, which can cause serious environmental problems. Among various released chemicals, the mercury(II) ion (Hg^{2+}) is classified as a persistent, bio-accumulative, and toxic chemical, and is considered a threat to humans and the environment.[1] Although Hg^{2+} is colourless, tasteless, and odourless, it can be easily absorbed into the body through the cell membranes of the skin, respiratory tract, and gastrointestinal tract.[2] The assimilation of Hg^{2+} in the human body can damage the central nervous system, endocrine glands, and organs.[3,4] Furthermore, chronic exposure to Hg^{2+} has been associated with various diseases, such as Minamata disease, acrodynia, Alzheimer's disease, and Hunter–Russell syndrome.[5] Consequently, the U.S. Environmental Protection Agency (EPA) has recommended that the maximum level of inorganic mercury in drinking water is 10 nM.[6] The common methods employed for the detection of Hg^{2+} include inductively coupled plasma atomic emission spectroscopy (ICP-AES),[7] atomic absorption spectroscopy,[8,9] electrochemical

analysis,[10–12] surface-enhanced Raman spectroscopy (SERS),[13,14] piezoelectric detection,[15] and colourimetric and fluorometric detection.[16] In particular, fluorescent chemosensors for Hg^{2+} have been developed based on the Hg^{2+}-catalysed reaction and coordination of heteroatoms with Hg^{2+}.[17] However, these detection methods are very expensive and time-consuming, and require skilled laboratory professionals. Furthermore, they require bulky and fragile instrumental setup, including an additional optical source.

Electrochemiluminescence (ECL) is a luminescence process involving sequential electron transfers between electrogenerated species on an electrode surface.[18] Compared with the photoluminescence (PL) process, ECL offers several advantages due to its low background signal and high sensitivity. In addition, ECL rarely requires complicated procedures, complex conditions, or bulky equipment for analysis.[18–20] Consequently, ECL has been considered a powerful tool for real-time, on-site sample analysis, and several studies have reported systems that combine the ECL technique with chemosensors.[21–41] So far, most ECL molecular probes have been developed using tris(2,2′-bipyridine)ruthenium(II) complexes ([Ru(bpy)$_3$$^{2+}$]) with their characteristically low metal-centred state (MC state), making it challenging to adjust the wavelength with changes in the molecular structure.[42] Among various luminophores considered as replacements for Ru(II) complexes, Ir(III) complexes are regarded as promising ECL

Department of Chemistry, Seoul National University, 1 Gwanak-ro, Gwanak-gu, Seoul 151-747, Korea. E-mail: jihong@snu.ac.kr

†Electronic supplementary information (ESI) available. See DOI: https://doi.org/10.1039/d3an01266b

luminophores due to their high ECL quantum yields and colour tunability through ligand modification by high ligand field stabilization energies.[33,43–48] Hong and co-workers reported the first ECL analysis system for the detection of Hg^{2+} ions based on the reaction of a small molecular probe with these ions.[35] Unfortunately, this system could not be applied in field monitoring because large amounts of organic solvents were required. Consequently, the development of new ECL probes with high selectivity and sensitivity toward Hg^{2+} in aqueous solutions is greatly desired.

Herein, we report a new PL and ECL chemodosimetric probe based on an iridium(III) complex for the determination of Hg^{2+} (Scheme 1). The design strategy of probe **1** is based on the following: (i) [Ir(piq)$_2$(bpy)][PF$_6$] (piq = 1-phenylisoquino-line, bpy = bipyridine) was selected as a luminophore, and (ii) *o*-aminomethylphenylboronic acid was introduced into the ancillary ligand as a PL and ECL signalling modulator, as well as a reaction site for the Hg^{2+} ions.[49–53] Probe **1** was expected to exhibit significant PL and ECL changes towards Hg^{2+} ions in aqueous solutions when compared to other Ir(III)-based

probes because this probe has cationic charge and hydrophilic *o*-aminomethylphenylboronic acid, which imparts high solubility in aqueous solutions. Probe **1** promptly reacted with Hg^{2+} ions through the transmetalation reaction to generate **1**-Hg^{2+}, resulting in decreased PL and ECL signals. Probe **1**, as analysed through PL and ECL, exhibited high sensitivity and selectivity in detecting Hg^{2+} ions within 2 min in aqueous solutions with small amounts of organic solvent (10% aceto-nitrile). These results imply significant potential for on-site Hg^{2+} detection, compared with other PL-based chemodosi-meters, as illustrated in Table S1.† In addition, probe **1** was successfully applied to ECL analysis of Hg^{2+} ions in tap water samples.

Experimental

Probes **1** and **2** were synthesised as shown in Scheme 2. Detailed synthetic procedures for compounds **1–11** are provided in the ESI.†

Scheme 1 The detection mechanism of probe **1** for Hg^{2+} ions.

Scheme 2 Synthetic routes of (a) compound **7**, (b) compound **8**, and (c) probes **1** and **2**.

Synthesis of 1

A mixture of crude compound **11** (17 mg, 20 μmol), compound **8** (7 mg, 25 μmol), and potassium carbonate (13 mg, 94 μmol) in 0.2 mL of acetonitrile was stirred at room temperature for 12 h. The solvent was evaporated under reduced pressure and extracted with dichloromethane three times. The organic phase was washed with water and brine, dried over anhydrous sodium sulphate, and evaporated. The residue was purified by silica gel column chromatography (acetonitrile/H_2O/sat. KNO_3(aq) = 40 : 4 : 1). The product was re-dissolved in dichloromethane/methanol (1 : 1, 1 mL) and stirred at room temperature for 2 h with potassium hexafluorophosphate (37 mg, 0.2 mmol). The solution was filtered, and the filtrate was evaporated under reduced pressure. The residue was triturated with dichloromethane and diethylether. The resulting precipitate was filtered, washed with diethylether and dried *in vacuo* to afford **1** (10 mg, 47%). ^1H NMR (300 MHz, $CDCl_3$) δ 8.99–8.84 (m, 2H), 8.78 (d, J = 8.2 Hz, 1H), 8.60 (s, 1H), 8.44 (s, 2H), 8.28–8.20 (m, 2H), 8.10 (t, J = 7.3 Hz, 1H), 7.89 (dd, J = 6.2, 3.0 Hz, 2H), 7.80–7.69 (m, 6H), 7.64 (d, J = 5.6 Hz, 1H), 7.40–7.28 (m, 8H), 7.22 (d, J = 7.1 Hz, 1H), 7.10 (t, J = 7.6 Hz, 2H), 6.88 (t, J = 7.0 Hz, 2H), 6.25 (d, J = 7.3 Hz, 2H), 3.82 (d, J = 5.5 Hz, 4H), 2.28 (s, 3H). ^{13}C NMR (126 MHz, CD_3CN) δ 168.49, 168.45, 156.01, 155.25, 153.47, 153.38, 150.68, 150.61, 145.57, 145.53, 140.80, 140.68, 139.47, 137.09, 137.07, 135.92, 131.98, 131.87, 130.86, 130.83, 130.75, 130.57, 130.50, 129.14, 129.02, 129.01, 128.64, 128.48, 127.56, 127.54, 127.45, 126.76, 126.75, 126.17, 126.15, 125.63, 124.86, 122.32, 122.30, 121.98, 121.90, 62.75, 58.55, 40.79. LRMS (MALDI-TOF) *m/z*: [M]$^+$ calc. for $C_{49}H_{40}BIrN_5O_2$ 934.290, found 934.063. HRMS (FAB) *m/z*: [M − H_2O]$^+$ calc. for $C_{49}H_{38}BIrN_5O$ 916.2799, found 916.2793.

Synthesis of 2

A mixture of crude compound **11** (9 mg, 11 μmol), benzyl bromide (4 mg, 23 μmol), potassium iodide (4 mg, 24 μmol), and potassium carbonate (3 mg, 22 μmol) in 0.2 mL of acetonitrile was stirred at room temperature for 12 h. The solvent was evaporated under reduced pressure and extracted with dichloromethane three times. The organic phase was washed with water and brine, dried over anhydrous sodium sulphate, and evaporated. The residue was re-dissolved in dichloromethane/methanol (1 : 1, 1 mL) and stirred at room temperature for 2 h with ammonium hexafluorophosphate (18 mg, 0.11 mmol). The solution was filtered and evaporated, and the residue was purified by silica gel column chromatography (CH_2Cl_2/MeOH = 50 : 1) to afford **2** (6 mg, 53%). ^1H NMR (400 MHz, $CDCl_3$) δ 8.92 (dd, J = 5.9, 3.1 Hz, 2H), 8.73 (d, J = 8.2 Hz, 1H), 8.58 (s, 1H), 8.26 (d, J = 8.0 Hz, 2H), 8.15 (t, J = 7.8 Hz, 1H), 7.90 (dd, J = 6.3, 3.1 Hz, 2H), 7.77 (dd, J = 6.4, 3.2 Hz, 4H), 7.72 (d, J = 4.9 Hz, 1H), 7.63 (d, J = 5.4 Hz, 1H), 7.49 (d, J = 20.2 Hz, 1H), 7.36 (m, J = 6.5 Hz, 7H), 7.28 (d, J = 7.3 Hz, 2H), 7.20 (d, J = 6.8 Hz, 1H), 7.11 (t, J = 7.6 Hz, 2H), 6.89 (t, J = 7.4 Hz, 2H), 6.27 (t, J = 6.6 Hz, 2H), 3.70 (d, J = 72.2 Hz, 4H), 2.26 (s, 3H). ^{13}C NMR (125 MHz, $CDCl_3$) δ 169.04, 168.99, 155.65, 155.47, 153.55, 153.41, 150.11, 145.47, 145.41, 140.21, 139.71,

136.99, 132.17, 131.70, 130.87, 130.85, 130.68, 130.66, 128.70, 128.49, 127.99, 127.59, 127.57, 126.93, 126.88, 126.31, 126.26, 125.38, 122.29, 121.98, 121.96, 62.03, 29.68. HRMS (FAB) *m/z*: [M]$^+$ calc. for $C_{49}H_{39}IrN_5$ 890.2835, found 890.2834.

Results and discussion

Spectroscopic properties of 1

We checked the changes in the UV-vis and PL spectra of probe **1** in the presence and absence of Hg^{2+} in an aqueous medium (pH 7.4, HEPES buffer/CH_3CN = 9 : 1, v/v). Probe **1** displayed an intense absorption peak at 288 nm, which was attributed to the spin-allowed ligand-centred (^1LC) transition states (Fig. S1†). Furthermore, the broad absorption peak detected around 330–510 nm was attributed to the mixing of metal-to-ligand charge-transfer (^1MLCT and ^3MLCT) transitions, ligand-centred (^3LC) transitions, and ligand-to-ligand charge-transfer (^3LLCT and ^1LLCT) transitions.[54] When the concentration of Hg^{2+} ions in solution increased, the absorption bands of probe **1** showed a slight red-shift. Subsequently, the PL response of probe **1** to Hg^{2+} was evaluated. As the amount of Hg^{2+} increased, the PL signal (λ_{ex} = 400 nm) gradually decreased until it reached a plateau after the addition of 10 μM Hg^{2+} (Fig. 1a). This indicated that probe **1** reacted in 1 : 1 stoichio-
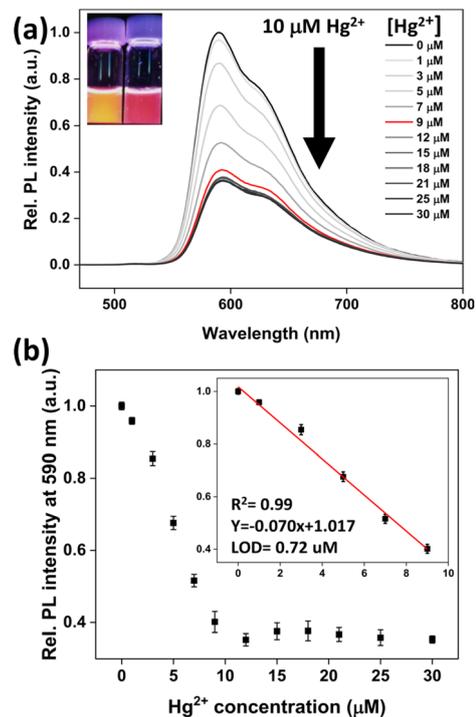

Fig. 1 (a) PL emission spectra (λ_{ex} = 400 nm) of probe **1** (10 μM) with increasing Hg^{2+} ion concentrations in CH_3CN/H_2O (1 : 9 v/v, pH 7.4, 10 mM HEPES). Inset: photographs of the probe solutions without and with Hg^{2+} under 365 nm UV irradiation. (b) PL intensity changes of probe **1** at 590 nm upon the addition of Hg^{2+} ions. Inset: a linear correlation between the PL intensity at 590 nm and the concentration of Hg^{2+}.

metry with Hg^{2+}. The limit of detection (LOD) was 0.73 μM from the linear correlation (R^2 = 0.99) between the concentration of Hg^{2+} ions (in the range of 0–10 μM) and the PL intensity (Fig. 1b).

To further understand the quenching behaviour of probe **1** in the presence of Hg^{2+}, its fluorescence lifetimes before and after the addition of Hg^{2+} ions were measured by time-correlated single-photon counting, whereby this probe exhibited single-exponential decay with a lifetime of 0.82 μs (Fig. S2a†). However, in the presence of Hg^{2+} ions, an additional shorter lifetime of ~0.1 μs was observed, thus revealing double-exponential decay in the PL decay curve. This can be attributed to the generation of the reaction product, **1**-Hg^{2+}, *via* the transmetalation reaction between Hg^{2+} and boronic acid on the ancillary ligands. Upon the addition of Hg^{2+}, the lifetimes decreased, thus indicating that the quenching mechanism was highly dependent on dynamic quenching (Fig. S2b†).[55–57] These changes were observed with the addition of up to 10 μM Hg^{2+} ions, which were consistent with the signal change trends observed in the PL response experiments.

To determine the selectivity of probe **1** in an aqueous solution, the PL spectra were measured in the presence of various metal ions. As expected, the PL of probe **1** decreased effectively only in the presence of Hg^{2+}, whereas other metal ions exhibited negligible PL signal changes (Fig. 2). This selectivity can be attributed to the transmetalation between phenylboronic acid and Hg^{2+} ions.[49–53] The PL of **1**-Hg^{2+} generated through the

reaction between probe **1** and Hg^{2+} was quenched by the electron transfer from the excited Ir(III) complex to Hg^{2+}.[58]

To investigate the probe's pH susceptibility, the PL intensity of probe **1** was measured in the pH range of 4–10 after the addition of Hg^{2+} (Fig. 3a). The probe showed a significant change in PL in the presence of Hg^{2+} over a wide pH range of 5–9, thus confirming its high stability in the detection of Hg^{2+}. The relatively weaker Hg^{2+} responses observed at pH 4 and 10 were presumably due to inefficient formation of boronate and generation of mercury(II) hydroxide, respectively.[59,60] Subsequently, the sensing ability toward Hg^{2+} ions in different ratios of CH$_3$CN–HEPES buffer solution was evaluated (Fig. 3b). Upon increasing the ratio of the HEPES buffer solution in the CH$_3$CN–HEPES buffer solution, a remarkable PL signal change in the presence of Hg^{2+} was observed since in an aqueous solution *o*-aminomethylphenylboronic acid undergoes H$_2$O insertion to generate boronate.[60] Since the formation of boronate is essential in a transmetalation reaction,[61–63] the reaction of probe **1** with Hg^{2+} ions occurred more efficiently in solutions with high H$_2$O content. Therefore, a significant PL response of probe **1** toward Hg^{2+} was induced in a 1:9 CH$_3$CN–HEPES buffer solution. The PL intensity of probe **1** was saturated within 2 minutes in the presence of 10 μM Hg^{2+} ions, indicating that Hg^{2+} ions could be detected quickly under our experimental conditions (Fig. S3†).

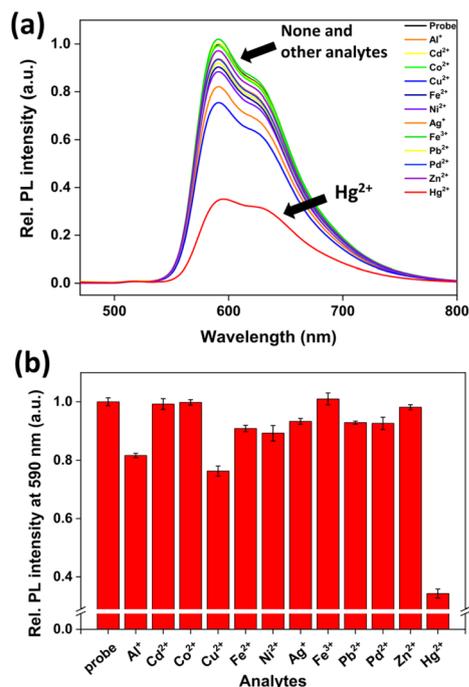**Fig. 2** (a) PL emission spectra (λ_{ex} = 400 nm) of probe **1** (10 μM) in the presence of various analytes (40 μM each; Hg^{2+}, 20 μM) in CH$_3$CN/H$_2$O (1:9 v/v, pH 7.4, 10 mM HEPES). (b) PL emission intensities at 590 nm of probe **1** (10 μM) upon the respective addition of various metal ions (40 μM).

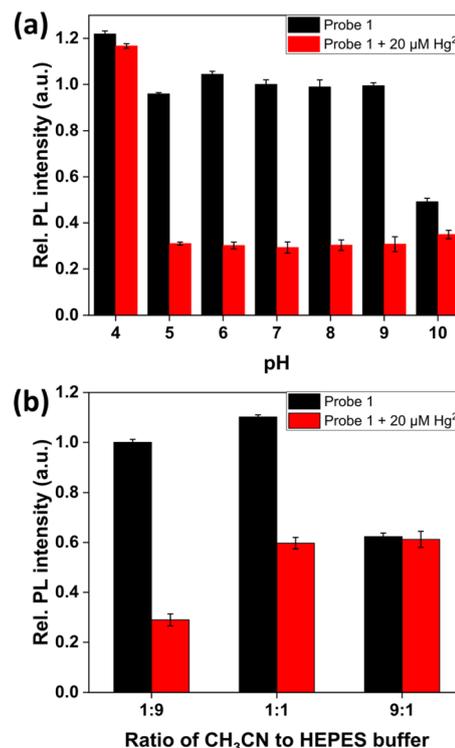**Fig. 3** PL intensity changes of probe **1** (10 μM, λ_{em} = 590 nm, λ_{ex} = 400 nm) towards 20 μM Hg^{2+} ions (a) in CH$_3$CN/H$_2$O (1:9 v/v, pH 7.4, 10 mM HEPES) under varying pH conditions and (b) in different ratios of CH$_3$CN to 10 mM HEPES buffer solution (pH = 7.40).

Proposed sensing mechanism

[1]H nuclear magnetic resonance (NMR) experiments with probe **1** in CD$_3$CN/D$_2$O (1:1) were then conducted (Fig. S4†). Upon the addition of Hg^{2+} ions to probe **1**, the signals at 3.75 ppm corresponding to the two methylene protons connected to the tertiary nitrogen were slightly downfield-shifted because of the binding of Hg^{2+} and the tertiary amine. However, after the addition of an excess amount of Hg^{2+} ions, the proton signals significantly decreased, and two new methylene proton peaks appeared at 3.72 and 3.53 ppm due to the reaction between boronic acid and Hg^{2+} ions. Similarly, the methyl proton signal at 2.25 ppm moved gradually downfield with the addition of Hg^{2+} ions with a decreased intensity, while a new peak appeared at 2.21 ppm with an increased intensity. High-performance liquid chromatography coupled with Thermo Scientific linear ion trap-orbitrap mass spectrometry (HPLC-LTQ-orbitrap) analysis was performed to confirm the reaction product generated after the addition of Hg^{2+} ions (Fig. S5†). Before the addition of Hg^{2+} ions, an m/z signal appeared at 934.6, which was attributed to probe **1**. Upon the addition of 20 μM Hg^{2+} ions to probe **1**, the m/z signal of probe **1** disappeared, and a major peak at 1115.6 appeared, which was attributed to **1**-Hg^{2+}. Both NMR and HPLC-LTQ-orbitrap analyses confirmed that probe **1** reacted effectively with Hg^{2+} through transmetalation to generate **1**-Hg^{2+}.

To confirm the role of boronic acid in the PL and ECL signal changes with Hg^{2+} ions, probe **2** without boronic acid was designed. The PL of probe **1** significantly decreased in the presence of 20 μM Hg^{2+} ions, while probe **2** hardly showed any PL changes, even after the addition of an excess amount of Hg^{2+} ions (Fig. 4). These results indicated that the transmetalation of boronic acid with Hg^{2+} ions is essential in the PL/ECL sensing mechanism.

To verify the signal changes in PL, an electrochemical analysis with DPV was performed (Fig. S6 and Table S2†). The highest occupied molecular orbital (HOMO) and lowest unoccupied molecular orbital (LUMO) energy levels of probe **1** were calculated to be −5.78 and −3.12 eV, respectively. Meanwhile, a mixture of probe **1** and 10 μM Hg^{2+} ions revealed a new peak at −0.54 V ($vs.$ Fc/Fc$^+$), which was attributed to the LUMO energy level (−4.26 eV) of –Hg$^+$, while the HOMO and LUMO energy levels of the Ir(III) complex were similar to those of probe **1**. The LUMO energy level of –Hg$^+$ lies between the HOMO and LUMO levels of the Ir(III) complex (Fig. S7†), which indicated that the PL signals of probe **1** were restrained by the photo-induced electron transfer (PeT) process from the Ir(III) complex to –Hg$^+$. Therefore, probe **1** showed decreased PL signals in the presence of Hg^{2+}. Meanwhile, **1**-Hg^{2+} showed a more stabilised LUMO energy level by 0.13 eV compared to probe **1** due to the mercury cation introduced into probe **1** through the transmetalation reaction. These results are in accordance with the red-shift tendency observed in the UV-vis absorption spectra of probe **1** with Hg^{2+} ions (Fig. S1†).
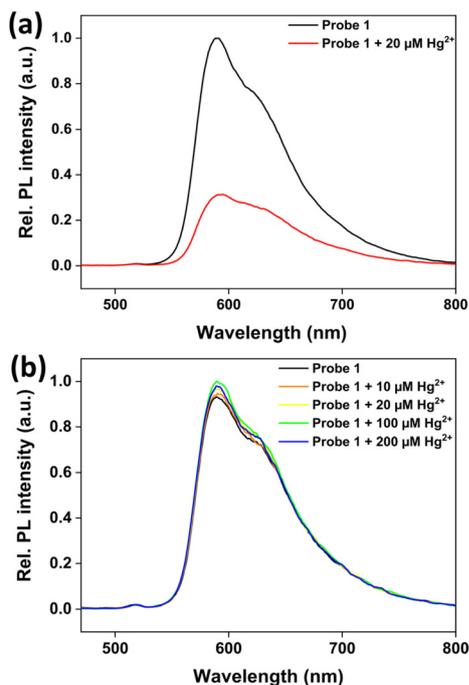

Fig. 4 PL intensity changes of (a) probe **1** and (b) probe **2** (10 μM) upon the addition of Hg^{2+} ions in CH$_3$CN/H$_2$O (1:9 v/v, pH 7.4, 10 mM HEPES).
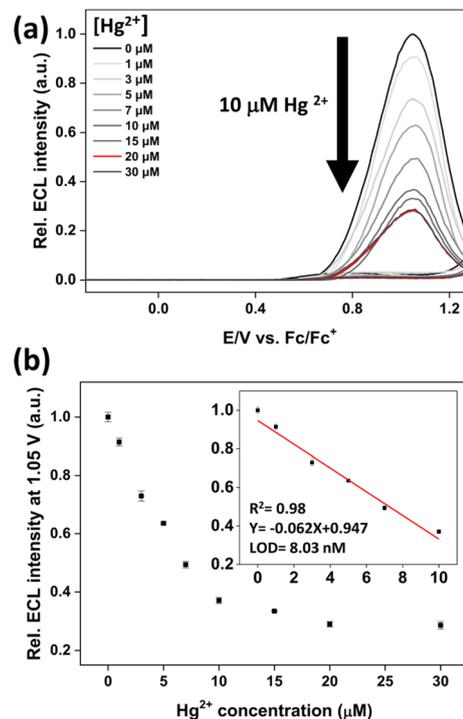
Fig. 5 (a) ECL intensities of probe **1** (10 μM) upon the addition of Hg^{2+} in CH$_3$CN/H$_2$O (1:9 v/v, pH 7.4, 100 mM DBAE, 0.1 M HEPES, 0.1% polidocanol and 0.1 M TBAP as the supporting electrolyte) while the potential is swept at a GC disk electrode (diameter 2 mm) in the range of −0.3–1.3 V (scan rate: 0.1 V s^{-1}). (b) ECL intensity changes of probe **1** at 1.05 V upon the addition of Hg^{2+}. Inset: a linear correlation between the ECL intensity at 1.05 V and the concentration of Hg^{2+}.
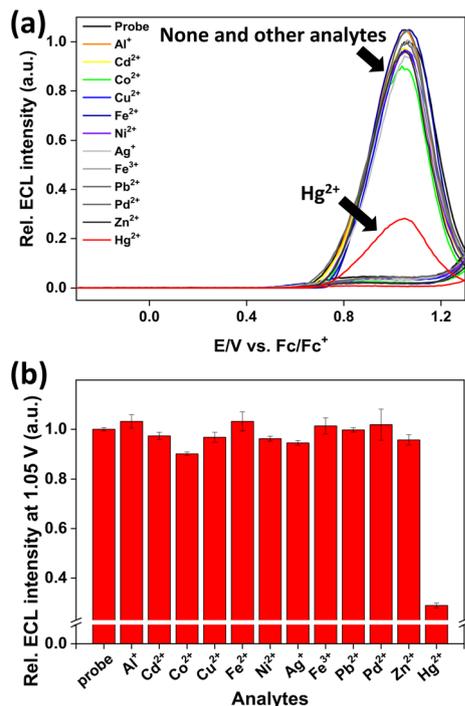
Fig. 6 (a) ECL intensities of probe **1** (10 μM) in the presence of various metal ions (40 μM each; Hg²⁺ 20 μM) in CH₃CN/H₂O (1 : 9 v/v, pH 7.4, 100 mM DBAE, 0.1 M HEPES, 0.1% polidocanol, and 0.1 M TBAP as the supporting electrolyte) while the potential is swept at a GC disk electrode (diameter 2 mm) in the range of −0.3–1.3 V (scan rate: 0.1 V s⁻¹). (b) ECL intensities at 1.05 V of probe **1** (10 μM) upon the respective addition of various metal ions (40 μM) and Hg²⁺ ions (20 μM).

ECL properties of 1

Fig. 5a shows the ECL emission profile during cyclic voltammetry in aqueous media (pH 7.4, HEPES buffer/CH₃CN = 9 : 1 v/v, 0.1 M 2-(dibutylamino)ethanol (DBAE), 0.1 M HEPES, 0.1%

polidocanol, and 0.1 M tetrabutylammonium perchlorate (TBAP) as the supporting electrolyte). Probe **1** produced a strong ECL signal around 1.05 V. However, the ECL signals gradually decreased as the amounts of Hg²⁺ increased. Interestingly, the ECL signals showed a linear correlation with Hg²⁺ concentrations in the range of 0–10 μM (Fig. 5b, R^2 = 0.98) with a LOD of 8.03 nM, which was much lower than the LOD determined by the PL method. This value falls below the maximum allowable contaminant level of mercury in drinking water recommended by the U.S. EPA. The high sensitivity of probe **1** demonstrates its ability to effectively detect Hg²⁺ ions in waste streams, which can have significant adverse effects on the environment.

As shown in Fig. 6, the ECL intensity of probe **1** did not show any significant changes upon the addition of other metal ions; however, a significant decrease in the ECL signal (~20% that of probe **1**) was observed after the addition of 20 μM (2 equiv.) of Hg²⁺. The designed system showed rapid reaction rate, high sensitivity, and remarkable selectivity toward Hg²⁺ ions, thus offering a new practical method for field monitoring of Hg²⁺ ions.

Consequently, probe **1** can be used as a highly selective Hg²⁺ probe based on ECL analysis (Scheme 3). Probe **1** was directly oxidised on glassy carbon (GC) electrodes to form **1**˙⁺. Subsequently, it was turned into the excited state, **1***, by one-electron transfer from the DBAE radical (DBAE˙), which emitted red ECL. In the presence of Hg²⁺, probe **1** rapidly reacted with Hg²⁺ via an irreversible transmetalation reaction to generate **1**-Hg²⁺. The excited state of **1**-Hg²⁺ was formed via a mechanism similar to that of probe **1** when oxidation occurs on the GC electrode. However, (**1**-Hg²⁺)* was rapidly consumed through an immediate PeT process from (**1**-Hg²⁺)* to −Hg⁺, resulting in a significant decrease in the ECL intensity (Fig. S7†).
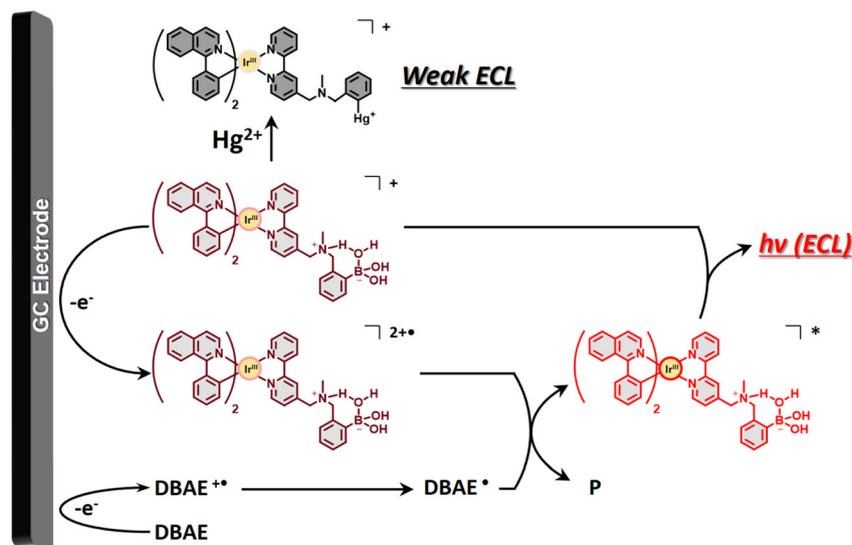
Scheme 3 The proposed sensing mechanism of probe **1** for detection of Hg²⁺ ions through ECL analysis.

Table 1 Quantification of Hg^{2+} in tap water samples[a]

[Hg^{2+}]$_{added}$[b]	Rel. ECL intensity (experiment, n = 3)	[Hg^{2+}]$_{calc'd}$ (μM)	Recovery (%)
0 μM	1 ± 0.0167	—	—
3 μM	0.7514 ± 0.0028	3.1780 ± 0.0347	105.93 ± 1.10
5 μM	0.6371 ± 0.0071	5.0356 ± 0.1145	100.71 ± 2.27
7 μM	0.5277 ± 0.0040	6.8137 ± 0.0655	97.34 ± 0.96
10 μM	0.3409 ± 0.0068	9.8500 ± 0.1107	98.50 ± 1.12

[a] All ECL intensities were measured along with the cyclic voltammetry (CV) scan in CH$_3$CN/H$_2$O (1 : 9 v/v, pH 7.4, 100 mM DBAE, 0.1 M HEPES, 0.1% polidocanol, and 0.1 M TBAP) while the potential was swept at a GC working electrode in the range of −0.3–1.3 V vs. Fc/Fc$^+$. [b] Concentrations of Hg^{2+} ions in tap water samples.

Quantification of Hg^{2+} ions in tap water

To confirm the reliability of the ECL sensing system in real samples, probe **1** was used to quantify Hg^{2+} ions in tap water using the standard addition method. Analytical solutions were prepared by diluting 1 mL of tap water containing varying concentrations of Hg^{2+} ions with 1 mL of CH$_3$CN/H$_2$O (1 : 4 v/v, pH 7.4, 20 μM probe **1**, 200 mM DBAE, 0.2 M HEPES, 0.2% polidocanol, and 0.2 M TBAP). Hg^{2+} ions in the diluted analytical solutions were quantified by comparing ECL values with the calibration curve shown in Fig. 5b. Then, the actual concentrations of Hg^{2+} ions in tap water samples were accurately determined by multiplying the values obtained from the calibration curve by the dilution factor of **2**. First, the ECL emission of probe **1** in tap water was assessed and almost no change in the ECL signal occurred prior to the addition of Hg^{2+} (Table 1). This observation was made in comparison with the ECL intensity of probe **1** in CH$_3$CN/H$_2$O (as shown in the inset of Fig. 5b), suggesting that the tap water sample contained a negligible amount of Hg^{2+}. As the concentration of Hg^{2+} ions increased, the ECL signal of probe **1** decreased. The recovery rates for Hg^{2+} ions ranged from 97.34% to 105.93%, indicating the high reliability and feasibility of this system for the detection of Hg^{2+} in actual environmental samples.

Conclusions

In summary, we developed a novel photoluminescent (PL) and electrochemiluminescent (ECL) dual signalling probe based on an Ir(III) complex with boronic acid as the reaction site for the selective detection of Hg^{2+} ions. PL and ECL analyses with the probe showed it had remarkable selectivity for Hg^{2+} ions with limits of detection of 0.72 μM and 8.03 nM, respectively. Furthermore, the successful quantification of Hg^{2+} ions in tap water samples using the ECL analysis demonstrated the effectiveness of this probe. Consequently, our system serves as a new proof-of-concept for real-time and on-site sample analysis. We believe that our strategy would be of great help to the advancement of developing ECL-based probes and other fields concerning ECL-based analysis.

Conflicts of interest

There are no conflicts to declare.

Acknowledgements

References

1 C. Kumunda, A. S. Adekunle, B. B. Mamba, N. W. Hlongwa and T. T. I. Nkambule, *Front. Mater.*, 2021, **7**, 616787.
2 B.-J. Ye, B.-G. Kim, M.-J. Jeon, S.-Y. Kim, H.-C. Kim, T.-W. Jang, H.-J. Chae, W.-J. Choi, M.-N. Ha and Y.-S. Hong, *Ann. Occup. Environ. Med.*, 2016, **28**, 5–5.
3 J. Mutter, J. Naumann, C. Sadaghiani, R. Schneider and H. Walach, *Neuroendocrinol. Lett.*, 2004, **25**, 331–339.
4 M. V. Yigit, A. Mishra, R. Tong, J. Cheng, G. C. L. Wong and Y. Lu, *Chem. Biol.*, 2009, **16**, 937–942.
5 A. Anandababu, S. Anandan and M. Ashokkumar, *ChemistrySelect*, 2018, **3**, 4413–4420.
6 W.-L. Cui, Z.-H. Zhang, L. Wang, J. Qu and J.-Y. Wang, *Spectrochim. Acta, Part A*, 2022, **267**, 120516.
7 Z. Zhu, G. C. Y. Chan, S. J. Ray, X. Zhang and G. M. Hieftje, *Anal. Chem.*, 2008, **80**, 7043–7050.
8 H. Erxleben and J. Ruzicka, *Anal. Chem.*, 2005, **77**, 5124–5128.
9 S. Gil, I. Lavilla and C. Bendicho, *Anal. Chem.*, 2006, **78**, 6260–6264.
10 S. Gupta, R. Singh, M. D. Anoop, V. Kulshrestha, D. N. Srivastava, K. Ray, S. L. Kothari, K. Awasthi and M. Kumar, *Appl. Phys. A*, 2018, **124**, 737.
11 S.-J. Liu, H.-G. Nie, J.-H. Jiang, G.-L. Shen and R.-Q. Yu, *Anal. Chem.*, 2009, **81**, 5724–5730.
12 A. Moutcine and A. Chtaini, *Sens. Bio-Sens. Res.*, 2018, **17**, 30–35.
13 Y. Du, R. Liu, B. Liu, S. Wang, M.-Y. Han and Z. Zhang, *Anal. Chem.*, 2013, **85**, 3160–3165.
14 S. J. Lee and M. Moskovits, *Nano Lett.*, 2011, **11**, 145–150.
15 D. P. Ruys, J. F. Andrade and O. M. Guimarães, *Anal. Chim. Acta*, 2000, **404**, 95–100.
16 G. Chen, Z. Guo, G. Zeng and L. Tang, *Analyst*, 2015, **140**, 5400–5443.
17 H. Shuai, C. Xiang, L. Qian, F. Bin, L. Xiaohui, D. Jipeng, Z. Chang, L. Jiahui and Z. Wenbin, *Dyes Pigm.*, 2021, **187**, 109125.
18 M. M. Richter, *Chem. Rev.*, 2004, **104**, 3003–3036.
19 M. Hesari and Z. Ding, *J. Electrochem. Soc.*, 2015, **163**, H3116–H3131.
20 W. Miao, *Chem. Rev.*, 2008, **108**, 2506–2553.
21 M. Schmittel and H.-W. Lin, *Angew. Chem., Int. Ed.*, 2007, **46**, 893–896.

22 E. Berni, I. Gosse, D. Badocco, P. Pastore, N. Sojic and S. Pinet, *Chem. – Eur. J.*, 2009, **15**, 5145–5152.

23 W. Zhang, D. Zhao, R. Zhang, Z. Ye, G. Wang, J. Yuan and M. Yang, *Analyst*, 2011, **136**, 1867–1872.

24 J.-W. Oh, T. H. Kim, S. W. Yoo, Y. O. Lee, Y. Lee, H. Kim, J. Kim and J. S. Kim, *Sens. Actuators, B*, 2013, **177**, 813–817.

25 K. Chen and M. Schmittel, *Chem. Commun.*, 2014, **50**, 5756–5759.

26 P. Li, Z. Jin, M. Zhao, Y. Xu, Y. Guo and D. Xiao, *Dalton Trans.*, 2015, **44**, 2208–2216.

27 H. Li, A. C. Sedgwick, M. Li, R. A. R. Blackburn, S. D. Bull, S. Arbault, T. D. James and N. Sojic, *Chem. Commun.*, 2016, **52**, 12845–12848.

28 Y. Xu, L. Zhang, Y. Liu, Z. Jin, Q. Zhao, F. Yang and D. Xiao, *Biosens. Bioelectron.*, 2016, **77**, 182–187.

29 D. Han, M. Qian, H. Gao, B. Wang, H. Qi and C. Zhang, *Anal. Chim. Acta*, 2019, **1074**, 98–107.

30 F. Yuan, K. Hao, S. Sheng, T. H. Fereja, X. Ma, F. Liu, M. N. Zafar, B. Lou, H. Tian and G. Xu, *Electrochim. Acta*, 2020, **329**, 135117.

31 Y. Dai, Z. Zhan, L. Chai, L. Zhang, Q. Guo, K. Zhang and Y. Lv, *Anal. Chem.*, 2021, **93**, 4628–4634.

32 I.-S. Shin, S. W. Bae, H. Kim and J.-I. Hong, *Anal. Chem.*, 2010, **82**, 8259–8265.

33 H. J. Kim, K.-S. Lee, Y.-J. Jeon, I.-S. Shin and J.-I. Hong, *Biosens. Bioelectron.*, 2017, **91**, 497–503.

34 S.-Y. Kim, H. J. Kim and J.-I. Hong, *RSC Adv.*, 2017, **7**, 10865–10868.

35 H. Rhee, T. Kim and J.-I. Hong, *Dalton Trans.*, 2018, **47**, 3803–3810.

36 K.-R. Kim, H. J. Kim and J.-I. Hong, *Anal. Chem.*, 2019, **91**, 1353–1359.

37 T. Kim and J.-I. Hong, *ACS Omega*, 2019, **4**, 12616–12625.

38 J. Park, T. Kim, H. J. Kim and J.-I. Hong, *Dalton Trans.*, 2019, **48**, 4565–4573.

39 H. J. Kim, T. Kim and J.-I. Hong, *Sens. Actuators, B*, 2020, **307**, 127656.

40 T. Kim, H. J. Kim, I.-S. Shin and J.-I. Hong, *Anal. Chem.*, 2020, **92**, 6019–6025.

41 Y. Namkoong, J. Oh and J.-I. Hong, *Chem. Commun.*, 2020, **56**, 7577–7580.

42 H. Wei and E. Wang, *Luminescence*, 2011, **26**, 77–85.

43 J. M. Fernandez-Hernandez, E. Longhi, R. Cysewski, F. Polo, H.-P. Josel and L. De Cola, *Anal. Chem.*, 2016, **88**, 4174–4178.

44 E. Kerr, E. H. Doeven, D. J. D. Wilson, C. F. Hogan and P. S. Francis, *Analyst*, 2016, **141**, 62–69.

45 J. I. Kim, I.-S. Shin, H. Kim and J.-K. Lee, *J. Am. Chem. Soc.*, 2005, **127**, 1614–1615.

46 E. Longhi, J. M. Fernandez-Hernandez, A. Iordache, R. Fröhlich, H.-P. Josel and L. De Cola, *Inorg. Chem.*, 2020, **59**, 7435–7443.

47 Z. M. Smith, E. Kerr, E. H. Doeven, T. U. Connell, N. W. Barnett, P. S. Donnelly, S. J. Haswell and P. S. Francis, *Analyst*, 2016, **141**, 2140–2144.

48 Y. Zhou, K. Xie, R. Leng, L. Kong, C. Liu, Q. Zhang and X. Wang, *Dalton Trans.*, 2017, **46**, 355–363.

49 A. Chatterjee, M. Banerjee, D. G. Khandare, R. U. Gawas, S. C. Mascarenhas, A. Ganguly, R. Gupta and H. Joshi, *Anal. Chem.*, 2017, **89**, 12698–12704.

50 X. Guo, J. Huang, Y. Wei, Q. Zeng and L. Wang, *J. Hazard. Mater.*, 2020, **381**, 120969.

51 S. W. Lee, S. Y. Lee and S. H. Lee, *Tetrahedron Lett.*, 2019, **60**, 151048.

52 S. Subedi, L. N. Neupane, P. K. Mehta and K.-H. Lee, *Dyes Pigm.*, 2021, **191**, 109374.

53 S. Subedi, L. N. Neupane, H. Yu and K.-H. Lee, *Sens. Actuators, B*, 2021, **338**, 129814.

54 M. Lepeltier, B. Graff, J. Lalevée, G. Wantz, M. Ibrahim-Ouali, D. Gigmes and F. Dumur, *Org. Electron.*, 2016, **37**, 24–34.

55 J. R. Lakowicz, *Principles of fluorescence spectroscopy*, Springer, New York, 2006.

56 A. S. Tanwar, L. R. Adil, M. A. Afroz and P. K. Iyer, *ACS Sens.*, 2018, **3**, 1451–1461.

57 A. S. Tanwar, R. Parui, R. Garai, M. A. Chanu and P. K. Iyer, *ACS Meas. Sci. Au*, 2022, **2**, 23–30.

58 J. H. He, Y. Y. Cheng, T. Yang, H. Y. Zou and C. Z. Huang, *Anal. Chim. Acta*, 2018, **1035**, 203–210.

59 M. Tian, C. Wang, Q. Ma, Y. Bai, J. Sun and C. Ding, *ACS Omega*, 2020, **5**, 18176–18184.

60 X. Sun, B. M. Chapin, P. Metola, B. Collins, B. Wang, T. D. James and E. V. Anslyn, *Nat. Chem.*, 2019, **11**, 768–778.

61 A. J. J. Lennox and G. C. Lloyd-Jones, *Angew. Chem., Int. Ed.*, 2013, **52**, 7362–7370.

62 A. J. J. Lennox and G. C. Lloyd-Jones, *Chem. Soc. Rev.*, 2014, **43**, 412–443.

63 C. F. R. A. C. Lima, A. S. M. C. Rodrigues, V. L. M. Silva, A. M. S. Silva and L. M. N. B. F. Santos, *ChemCatChem*, 2014, **6**, 1291–1302.